Longitudinal density modulation and energy conversion in intense beams

J. R. Harris
Lawrence Livermore National Laboratory, Livermore, California 94551, USA

J. G. Neumann
Naval Research Laboratory, Washington, DC 20379, USA

K. Tian and P. G. O'Shea
Department of Electrical and Computer Engineering, University of Maryland, College Park, Maryland 20740, USA

(Received 7 August 2006; revised manuscript received 27 March 2007; published 8 August 2007)

Density modulation of charged particle beams may occur as a consequence of deliberate action, or may occur inadvertently because of imperfections in the particle source or acceleration method. In the case of intense beams, where space charge and external focusing govern the beam dynamics, density modulation may, under some circumstances, be converted to velocity modulation, with a corresponding conversion of potential energy to kinetic energy. Whether this will occur depends on the properties of the beam and the initial modulation. This paper describes the evolution of discrete and continuous density modulations on intense beams and discusses three recent experiments related to the dynamics of density-modulated electron beams.

DOI: 10.1103/PhysRevE.76.026402 PACS number(s): 52.59.Sa, 41.75.Fr, 71.45.Lr, 52.35.Lv

I. INTRODUCTION

Any physical system in which a displacement of matter results in a restoring force can generally support oscillations. The exact nature of the oscillations will depend on the details of the restoring force, but in all cases these oscillations are characterized by alternating states of high potential energy gradients and high kinetic energy.

In charged particle beams of sufficiently high density or sufficiently low velocity, the beam diameter is set by a balance between the space charge forces generated within the beam and the external focusing applied to the beam. Such beams are referred to as "intense" [1]. The space charge and external focusing forces each consist of a transverse component perpendicular to the direction of travel, and a longitudinal component parallel to the direction of travel. The space charge force is a function of the line charge density in the beam, while the focusing force is determined by the properties of the beam transport system. Density modulation of the beam corresponds to an alteration in the space charge field, and therefore to a change in the quantity and location of potential energy stored in the beam.

A beam may become density modulated in several ways. If the beam initially contains uniform density, an external alternating electric field may be applied to impart a position-dependent velocity to the particles. This velocity modulation causes a bunching of the beam, and is the well-known operating principle of the klystron [2]. Note that this bunching of the beam corresponds to a conversion between a state where energy is stored in a kinetic form (velocity modulated) and a state where energy is stored in a potential form (density modulated). This represents only one half of the oscillatory cycle—a beam which is initially modulated in density should be driven by space charge to become modulated in velocity.

For modern accelerators, modulation is generally not deliberately applied at the cathode, where space charge driven effects are most pronounced. However, modulation is often applied accidentally due to peculiarities of the particle source. This modulation will consist of both velocity and density modulation, but density modulation generally dominates. This density modulation may have direct consequences, by altering beam transport and acceleration requirements, and by serving as a source of electromagnetic radiation after acceleration; or it may convert to velocity modulation which may cause beam dispersion. In this paper, we discuss the generation of intense density-modulated beams, their evolution under space charge forces, and their consequences for accelerator system design.

II. GENERATION OF DENSITY-MODULATED BEAMS

Two techniques have been used by the authors for generating density-modulated electron beams: photomodulation [3–9] and gridded guns [8,10–12]. In photomodulation, an electron beam is produced (at least in part) using photoemission. The maximum amount of current that can be produced from a cathode using photoemission is governed by the photon-counting equation

$$i[A] = \frac{\lambda[\mu m]}{124} P[W] QE[\%], \tag{1}$$

where $i[A]$ is the current in amperes, $\lambda[\mu\mathrm{m}]$ is the wavelength of the light in microns, $P[\mathrm{W}]$ is the power in watts of the light incident on the cathode, and $QE[\%]$ is the quantum efficiency of the cathode material at the wavelength being used, expressed in percent [7]. If the cathode material being used is a prompt photoemitter, and the gun is operated far from the space charge limit, then the pulse shape of the electron beam produced will be the same as that of the laser light applied to the cathode. Note that because increasing the number of photons incident on the cathode increases the number of electrons produced, photomodulation results in a beam which is largely density modulated; some velocity modulation may also be present because the gun is not an

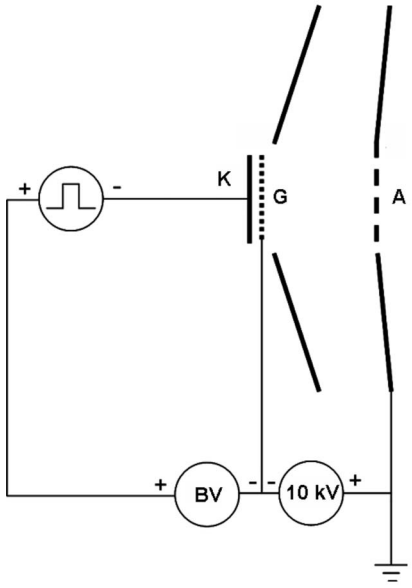

FIG. 1. Schematic of a gridded electron gun showing cathode (K), grid (G), anode (A), Pierce electrodes, grid bias voltage source (BV), cathode pulser source, and 10 kV accelerating potential [8].

ideal current source, but this will usually be a minor effect. Although the laser pulses used in photoinjectors are generally assumed to have "nice" pulse shapes, in practice they may contain structure which is poorly controlled and poorly diagnosed. This is particularly true in cases when the laser pulses are not transform limited. As a result, the electron beams produced often contain structure which cannot be controlled, but which can have an impact on beam transport, acceleration, and use. To study this mechanism for density modulation of beams in a controlled fashion, the laser beam may be deliberately modulated using several techniques, including systems of beam splitters and delay lines [7], or comb filters and related interferometry techniques [3,5]. As a result of these techniques, the density modulation applied to the beam can be very well controlled. If a dispenser photocathode [13] is used, additional control over beam shape is provided by the capability to simultaneously generate electrons using thermionic emission and photoemission. The range of pulse shapes that can be produced by these systems is governed by cathode temperature, type, and condition; laser power, frequency, and pulse shape; and space charge limits in the gun [9].

A second technique for generating density-modulated beams is the use of gridded guns. In these guns, a control grid is added to the basic gun diode, causing them to operate similar to triodes (Fig. 1). A bias voltage between the grid and cathode suppresses electron emission from the cathode, except during the cathode pulse. In this way, the grid is able to gate the output beam.

Both gridded guns and triodes may be operated in three regimes: saturation, amplification, and cutoff [2,8]. In saturation, space charge limits the current produced by the gun, and the current is governed by the Child-Langmuir equation. In this mode, the cathode-grid voltage has little effect on current. If the magnitude of the grid voltage is increased sufficiently, the current drawn from the cathode will begin to be suppressed, and the gun will be brought into triode amplification mode. In this mode, the current is governed by

$$J = K_T\left(V_G + \frac{V_A}{\mu}\right)^{3/2}, \tag{2}$$

where J is the current density produced from the cathode, K_T is a constant depending on the geometry of the gun, V_G is the voltage between the cathode and grid, and V_A is the voltage between the cathode and anode. The quantity μ is the amplification factor, which is a measure of the relative ability of the grid and anode voltages to control the current emerging from the cathode; μ is a function of the gun geometry [2]. In this mode, small changes in the cathode-grid voltage will produce large changes in the output current. If the grid voltage is adjusted so that

$$V_G + \frac{V_A}{\mu} \leqslant 0, \tag{3}$$

the gun will be driven into cutoff, and no current will escape the gun.

To deliberately produce a modulated beam, the gun is placed into triode amplification mode, and the cathode-grid voltage is modulated. Several techniques may be used to accomplish this, including pulse-forming lines [14] and radio-frequency modulating signals [15]. If the cathode-grid voltage is pulsed but the gun remains in triode amplification mode at the top of the gating pulse, then any ringing, droop, or other structure on the voltage pulse will be replicated in the current produced from the gun. Such structure is almost always present in the output signal of pulsed power systems.

The strengths of the velocity and density modulation produced by gridded guns can be calculated [8,16]. For a nonrelativistic beam produced from a gridded gun, density modulation will dominate as long as the accelerating voltage applied between the grid and anode is much greater than the control voltage applied between the grid and cathode. Therefore, in gridded guns, velocity modulation will be present, but density modulation will dominate.

Photomodulation and triode modulation are different, but complementary, techniques. Photoinjectors generally operate below the space charge limit, which allows the electron pulse shape to duplicate the laser pulse shape. Attempting to exceed the space charge limit will cause the onset of virtual cathode oscillations that cause the electron pulse shape to be very different than the laser pulse shape [17,18]. Gridded electron guns are generally designed to operate at the space charge limit; even if the gun as a whole is not operated at the space charge limit, the grid-cathode region will be, as it is this mechanism which allows the grid voltage to control the beam current [2]. Both techniques allow for precision control of electron pulse shapes. A photoinjector with an idealized pulse shape can produce beam pulses which simulate those produced from a gridded gun with a simple gating pulse applied to the grid. If the idealized photoinjector pulse is submodulated at higher frequency, the resulting pulse shape can simulate that from a gridded gun operating in triode amplification mode with a structured grid pulse. However,

photoinjectors typically have faster response times than gridded guns. In these systems, the limiting factor is generally the technique used for modulating the laser pulse, and modulation as high as terahertz frequencies has been demonstrated [6]. Modulation of gridded guns is typically limited to gigahertz frequencies and below, notably by electron transit time effects [2]. As a result, while gridded guns may be used to simulate beam configurations produced from photoinjectors under certain conditions, these will generally be scaled experiments.

III. EVOLUTION OF INTENSE DENSITY-MODULATED BEAMS

In the previous section, we described the generation of density-modulated beams and how the density modulation will be accompanied by a velocity modulation which is generally small. In this section, we will describe the evolution of these beams, and look at two experiments focusing on different aspects of this evolution.

A. Space charge waves

In intense beams, the longitudinal evolution is driven by space charge forces. The characteristic speed of this evolution is the "sound speed," which for electron beams is

$$c_0 = \sqrt{\frac{qg\lambda_0}{4\pi\varepsilon_0 m\gamma^5}}, \tag{4}$$

where q is the fundamental charge, λ_0 is the line charge density in the beam, ε_0 is the permittivity of free space, m is the mass of the electron, γ is the relativistic factor, and $g = \alpha + 2\ln\left(\frac{b}{a}\right)$ is a geometry factor depending on the beam diameter a and the beam pipe diameter b. The quantity α is generally taken to be zero or one, depending on the assumptions used [19]. This is the speed at which waves propagate in a beam [20], and determines the rate of longitudinal expansion of the beam [21]. Perturbations which are produced in beam velocity or density will generate a forward-traveling "fast wave" and a backward-traveling "slow wave," each traveling at c_0 in the beam frame (Fig. 2). Such perturbations have been investigated for use in beam diagnostics [22,23]. The behavior of these waves also depends on the strength of the current, density, and velocity perturbations and on the shape of the initial disturbance. For initial perturbations of the form

$$i_1(0,t) = \eta i_0 h(t), \tag{5}$$

$$\lambda_1(0,t) = (\eta - \delta)\lambda_0 h(t), \tag{6}$$

and

$$v_1(0,t) = \delta v_0 h(t), \tag{7}$$

the current, line charge density, and velocity will evolve according to

$$i_1(z,t) = -\frac{i_0}{2}\left[\delta\frac{v_0}{c_0} - \eta + (\eta-\delta)\frac{c_0}{v_0}\right]h\left(t - \frac{z}{v_0 - c_0}\right) + \frac{i_0}{2}\left[\delta\frac{v_0}{c_0} + \eta + (\eta-\delta)\frac{c_0}{v_0}\right]h\left(t - \frac{z}{v_0 + c_0}\right), \tag{8}$$

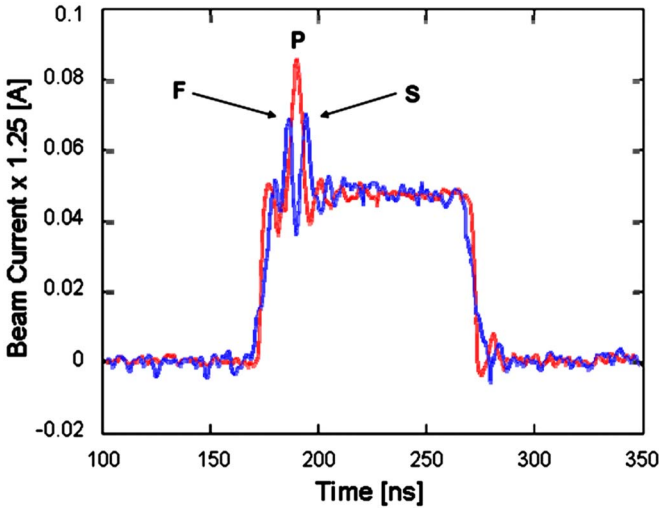

FIG. 2. (Color online) Beam current measured near the cathode and downstream during a photomodulation experiment with an intense electron beam in the University of Maryland Electron Ring. Initial perturbation (P) launches a forward-traveling fast wave (F) and a backward-traveling slow wave (S) [12].

$$\lambda_1(z,t) = -\frac{\lambda_0}{2}\left[\delta\frac{v_0}{c_0} - (\eta-\delta)\right]h\left(t - \frac{z}{v_0 - c_0}\right) + \frac{\lambda_0}{2}\left[\delta\frac{v_0}{c_0} + (\eta-\delta)\right]h\left(t - \frac{z}{v_0 + c_0}\right), \tag{9}$$

and

$$v_1(z,t) = +\frac{v_0}{2}\left[\delta - (\eta-\delta)\frac{c_0}{v_0}\right]h\left(t - \frac{z}{v_0 - c_0}\right) + \frac{v_0}{2}\left[\delta + (\eta-\delta)\frac{c_0}{v_0}\right]h\left(t - \frac{z}{v_0 + c_0}\right), \tag{10}$$

where $h(t)$ is a function varying between zero and one which describes the initial shape of the perturbation, and η and δ are quantities defining the strengths of the current and velocity modulations [20]. Note that the strengths of the initial density and velocity perturbations determine the relative strengths of the fast and slow waves, and that if these parameters are set properly, the disturbance on the beam can consist of only a single fast wave or only a single slow wave [20]. Conversely, the relative strengths of the fast and slow waves can be used as a diagnostic to reconstruct the relative strengths of the initial velocity and density perturbations which launched them.

B. Discrete perturbations

Recently, experiments have been performed on the Long Solenoid Experiment at the University of Maryland to study the evolution of discrete perturbations in intense beams [10,14]. In this experiment, a 5 keV electron beam is produced from a gridded, variable-perveance electron gun [24], and transported through a solenoid focusing channel to a high-resolution energy analyzer [25–27] 2.3 m downstream

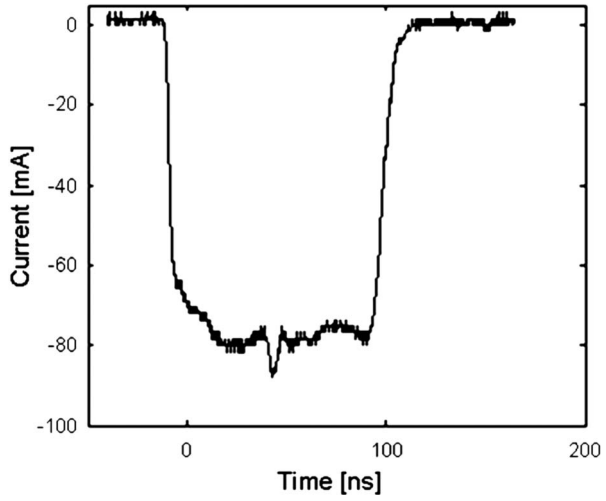

FIG. 3. Example of beam current modulation produced in a gridded electron gun [14].

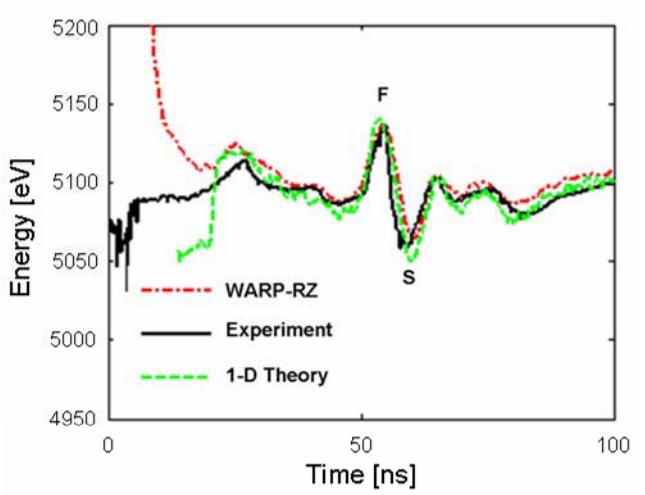

FIG. 4. (Color online) Average electron kinetic energy, as a function of position in beam, resulting from the perturbation shown in Fig. 3. Comparison of experiment, theory, and simulation shows good agreement in the region of the fast (F) and slow (S) waves [14].

from the gun. Emission from the electron gun is suppressed by applying a constant bias voltage between the grid and cathode, except during a nominal 100 ns long pulse produced by a pulse-forming line. To produce a density (dominated) perturbation in the beam, the pulse-forming line is modified by the addition of a T connector and stub line. A typical pulse shape is shown in Fig. 3. To adjust the pulse shape, the bias voltage applied between the grid and cathode is adjusted. As the gun is operating in triode-amplification mode, this results in a change in both the main beam current and the perturbation current. When the beam reaches the energy analyzer, the beam energy as a function of position is measured; for small initial perturbations, results are found to agree well with the one-dimensional theory of Eqs. (5)–(10), and with predictions from the WARP-RZ particle-in-cell code (Fig. 4). For comparison to theory, the initial velocity perturbation strength δ was set to zero, while the initial current perturbation strength η and the perturbation shape function $h(t)$ were directly captured from the current profiles in Fig. 3. For stronger perturbations, the theoretical assumption of small disturbances no longer holds, and higher-order terms would need to be included in the theory. (Photomodulation techniques have also been used to generate single perturbations; these experiments are discussed in more detail elsewhere [7–9,11,12,28].)

For theoretical purposes, let us now consider an idealized version of this experiment. The assumption of pure density modulation from a triode-type gun is not exact, but it is very close. Under this assumption, $\delta=0$ and the equations for the perturbed density, current, and velocity become

$$\lambda_1(z,t) = \frac{\lambda_0}{2}\eta h\left(t - \frac{z}{v_0 - c_0}\right) + \frac{\lambda_0}{2}\eta h\left(t - \frac{z}{v_0 + c_0}\right), \quad (11)$$

$$i_1(z,t) = \frac{i_0}{2}\left[\eta - \eta\frac{c_0}{v_0}\right]h\left(t - \frac{z}{v_0 - c_0}\right) + \frac{i_0}{2}\left[\eta + \eta\frac{c_0}{v_0}\right]h\left(t - \frac{z}{v_0 + c_0}\right), \quad (12)$$

and

$$v_1(z,t) = -\frac{c_0}{2}\eta h\left(t - \frac{z}{v_0 - c_0}\right) + \frac{c_0}{2}\eta h\left(t - \frac{z}{v_0 + c_0}\right). \quad (13)$$

This indicates that an initial density modulation of $\lambda_1(t=0) = \lambda_0\eta h(t=0)$ will spawn a fast and slow density wave, each of peak magnitude $\frac{\lambda_0}{2}\eta$, and a fast velocity wave of magnitude $\frac{c_0}{2}\eta$ and a slow velocity wave of magnitude $-\frac{c_0}{2}\eta$. This model's prediction of fast and slow velocity waves which retain the shape of the initial density perturbation, but have opposite polarities, agrees well with experimental observations from the long solenoid experiment [14]. We now consider the potential and kinetic energy stored in the perturbation and waves. The potential energy associated with a charge distribution is the energy stored in the resulting electric field

$$U = \frac{\varepsilon_0}{2}\int E^2 dV. \quad (14)$$

In the long wavelength limit and far from the beam ends, the electric field due to an intense beam consists of both a longitudinal component and a transverse component. The longitudinal component is given by [19]

$$E_z = \frac{-g}{4\pi\varepsilon_0\gamma^2}\frac{\partial\lambda}{\partial z}. \quad (15)$$

The transverse component is found (approximately, for the long-wavelength regime) from Gauss' Law, and is

$$E_\perp = \frac{\lambda}{2\pi\varepsilon_0 r} \quad (16)$$

between the beam and the beam pipe and

$$E_\perp = \frac{r\rho}{2\varepsilon_0} \tag{17}$$

inside the beam. Here g is the geometry factor previously discussed, λ is the local line charge density in the beam, r is the radial position, and ρ is the beam volume charge density. For an intense beam, the volume charge density in each slice of the beam is generally taken to be a constant, with changes in the line charge density being due to changes in the beam radius [29]

$$a = \sqrt{\frac{\lambda}{\pi\rho}}. \tag{18}$$

When this assumption is used in the derivation of the longitudinal electric field $\alpha=0$ and the electric field is found to be uniform across the beam cross section. Combining Eqs. (14)–(18), and integrating over the proper limits, the potential energy stored in the electric field of the beam, over a region of the beam between z_1 and z_2, is found to be

$$\begin{aligned} U = \varepsilon_0 \int_{z_1}^{z_2} \left[\frac{g}{4\pi\varepsilon_0\gamma^2} \frac{\partial\lambda_1(z)}{\partial z} \right]^2 \frac{\lambda_0 + \lambda_1(z)}{2\rho} dz \\ + \int_{z_1}^{z_2} \frac{[\lambda_0 + \lambda_1(z)]^2}{16\varepsilon_0\pi} dz \\ + \int_{z_1}^{z_2} \frac{[\lambda_0 + \lambda_1(z)]^2}{4\pi\varepsilon_0} \ln \frac{b\sqrt{\pi\rho}}{\sqrt{\lambda_0 + \lambda_1(z)}} dz. \end{aligned} \tag{19}$$

Here, it is assumed that the line charge density $\lambda(z)$ is the sum of an unperturbed value λ_0 and a perturbed value $\lambda_1(z)$. Note that the first term in Eq. (19) represents the energy stored in the longitudinal electric field of the beam, the second term represents the energy stored in the transverse field of the beam within the beam itself, and the third term represents the energy stored in the transverse field of the beam between the beam radius and the beam pipe. To find a simpler expression, we note that for small perturbations $\eta \ll 1$ and discard all terms carrying factors of η^2 or η^3. In addition, we discard $\lambda_1(z)$ in the logarithmic term in Eq. (19), as this will tend to have a very small effect on the overall stored energy. When this is done, the energy stored in the beam becomes

$$\begin{aligned} U = \int_{z_1}^{z_2} \frac{{\lambda_0}^2}{4\pi\varepsilon_0} \ln \frac{b\sqrt{\pi\rho}}{\sqrt{\lambda_0}} dz + \int_{z_1}^{z_2} \frac{{\lambda_0}^2}{16\varepsilon_0\pi} dz \\ + \int_{z_1}^{z_2} \frac{2\lambda_0\lambda_1(z)}{4\pi\varepsilon_0} \ln \frac{b\sqrt{\pi\rho}}{\sqrt{\lambda_0}} dz + \int_{z_1}^{z_2} \frac{2\lambda_0\lambda_1(z)}{16\varepsilon_0\pi} dz. \end{aligned} \tag{20}$$

However, for this paper, we are concerned with changes in stored energy, and so only terms depending on perturbed quantities are of interest. In this case, the perturbation in the stored energy becomes

$$U_1 = \frac{\lambda_0}{2\pi\varepsilon_0} \left[\frac{1}{4} + \ln \frac{b\sqrt{\pi\rho}}{\sqrt{\lambda_0}} \right] \int_{z_1}^{z_2} \lambda_1(z) dz. \tag{21}$$

Note that the longitudinal electric field does not contribute at all to this quantity, as it consisted of higher powers of η and was discarded. Therefore, regions of increased current in intense beams increase the beam radius and store additional energy in the transverse electric field of the beam. Also, note that the bracketed term in Eq. (21) depends on the ratio $\ln \frac{b\sqrt{\pi\rho}}{\sqrt{\lambda_0}} = \ln \frac{b}{a_0}$, and looks similar to a modified, average geometry factor corresponding to the unperturbed beam radius a_0; for simplicity, we write this term as g' in the equations that follow.

For a single perturbation, the additional potential energy stored in the initial perturbation is

$$U_i = \frac{\eta g' \lambda_0^2}{2\pi\varepsilon_0} \int_{\text{perturbation}} h(t) dz. \tag{22}$$

After some time, the fast and slow density waves have separated, and the final potential energy stored in the system can be calculated. In the case of a single, discrete initial perturbation, the line charge density $\lambda_1(z)$ will consist of two discrete perturbations, each preserving the width, shape, and half the height of the original density perturbation. Therefore, the final stored potential energy is

$$U_f = \frac{\eta g' \lambda_0^2}{2\pi\varepsilon_0} \left[\int_{\text{fast}} \frac{h(t)}{2} dz + \int_{\text{slow}} \frac{h(t)}{2} dz \right], \tag{23}$$

which is identical to the potential energy stored in the initial perturbation, given by Eq. (22).

If the potential energy stored in the perturbed beam does not change, what about the kinetic energy in the beam? The nonrelativistic kinetic energy for a distribution of particles is[1]

$$T = \frac{1}{2} \int v^2 dm \tag{24}$$

or

$$T = \frac{m}{2q} \int v^2 \lambda(z) dz. \tag{25}$$

For our beam, both the velocity and density consist of perturbed and unperturbed quantities, so

[1]This is the kinetic energy associated with the longitudinal motion of the particles only. Kinetic energy associated with transverse motion of the particles in the beam will be related to the square of the change in beam radius $(da/dz)^2$, which for an intense beam is related to the beam line charge density by $\{[2\sqrt{\lambda_0+\lambda_1(z)}]^{-1} d\lambda_1/dz\}^2$, which is essentially a higher order term carrying a factor of η^2. We may therefore disregard this contribution while being consistent with the other approximations in this paper.

$$T = \frac{m}{2q}\int [v_0 + v_1(z)]^2[\lambda_0 + \lambda_1(z)]dz. \tag{26}$$

The perturbed quantities each carry a factor of η; preserving only the terms of order η^0 or η^1, this becomes

$$T = \frac{m}{2q}\int [{v_0}^2\lambda_0 + {v_0}^2\lambda_1(z) + 2v_0v_1(z)\lambda_0]dz. \tag{27}$$

The first term is the kinetic energy carried by the unperturbed beam, and therefore is not associated with any evolution of the perturbations.

The second term is the added contribution to the beam's kinetic energy due to the added mass placed in the beam by the initial density modulation. This term can be rewritten as

$$T_{\Delta\lambda} = \frac{m{v_0}^2\lambda_0\eta}{4q}\left[\int_{\text{fast}} h\left(t - \frac{z}{v_0 + c_0}\right)dz + \int_{\text{slow}} h\left(t - \frac{z}{v_0 - c_0}\right)dz\right]. \tag{28}$$

For small initial perturbations, described by the first-order theory of Reiser, the shape of the fast and slow waves does not change over time, and is identical to the shape of the initial density perturbation. Thus, the integrals in Eq. (28) always sum to a constant, and $T_{\Delta\lambda}$ does not change.

The third term in Eq. (27) is the contribution of the perturbed velocity to the kinetic energy stored in the beam. This term may be rewritten as

$$T_{\Delta v} = \frac{mv_0c_0\lambda_0\eta}{2q}\left[\int_{\text{fast}} h\left(t - \frac{z}{v_0 + c_0}\right)dz - \int_{\text{slow}} h\left(t - \frac{z}{v_0 - c_0}\right)dz\right]. \tag{29}$$

Because the shapes of the fast and slow waves do not change over time, the integrals in Eq. (29) always sum to zero. As a result, there is no net contribution of the velocity disturbance to the kinetic energy stored in the beam. Therefore, in the case of discrete initial density perturbations, the excess potential and kinetic energy stored in the beam do not change over time, and there is no oscillation between density modulation and velocity modulation once the fast and slow waves have separated. Rather, the effect of waves launched from a discrete perturbation is to alter the location in the beam where excess energy is stored, rather than the form in which it is stored.

C. Periodic modulation

Density modulation can also be imposed on an intense beam in the form of a continuous, periodic modulation. Because any periodic modulation can be expressed as a combination of sines and cosines through the Fourier series, we will emphasize modulations of these types.

Experiments on continuous density modulation of intense beams at the University of Maryland have been performed on the University of Maryland Electron Ring (UMER).

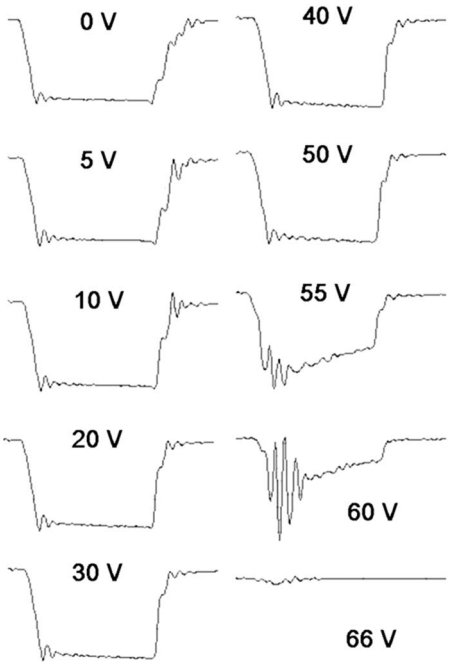

FIG. 5. UMER beam profile as a function of bias voltage measured 7.7 m downstream from the cathode [8].

UMER is a 10 keV, 100 mA strong-focusing electron beam transport system for the study of intense beam dynamics [1,30]. The beam in UMER is produced from a gridded electron gun with Pierce focusing [31,32]. As with the gun for the long solenoid experiment, emission from the UMER cathode is suppressed by applying a bias potential between the grid and cathode. To produce beam, a pulse-forming line is used to apply a pulse to the cathode, with the result that the potential between the grid and cathode is changed, allowing electrons to escape through the grid and be accelerated by the 10 kV accelerating potential (Fig. 1). Under normal conditions, the bias voltage is set to approximately 40 V, which ensures that the gun is driven into saturation during the cathode pulse but is kept in triode cutoff otherwise. However, by increasing the bias voltage to approximately 60 V, the gun will not be able to reach saturation, and instead will remain in triode amplification mode throughout the cathode pulse [8]. When this happens, the beam current pulse shape is no longer rectangular, but instead shows a pronounced sinusoidal modulation at the beam head, followed by an exponential decay in the remainder of the pulse. These current profiles are shown in Fig. 5, as measured on a beam position monitor (BPM) [33] 7.7 m downstream from the cathode. This modulation is believed to be due to triode amplification of structure present on the signal provided by the pulse-forming line. By adjusting the bias voltage to bring the gun into triode cutoff, the amplification factor of the UMER gun was measured to be 910. This value is large compared to the amplification factors typical for triode tubes, which generally range from about 2.5 to about 200 [2]. The size of the UMER amplification factor is due to its very large grid-anode spacing, which is between 170 and 270 times greater than the spacing between grid wires [8]. Even so, the measured amplification factor is less than the theoretical value of 1493

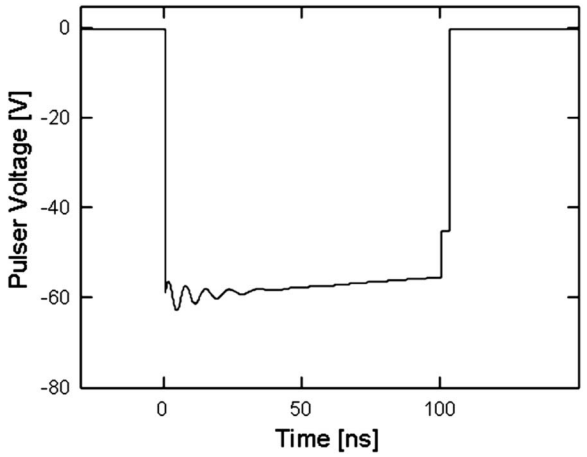

FIG. 6. Approximate UMER pulse-forming line signal [8]. This function was inferred using Eq. (2), which calculates output current waveforms very close to those measured experimentally when this function is used as the grid voltage.

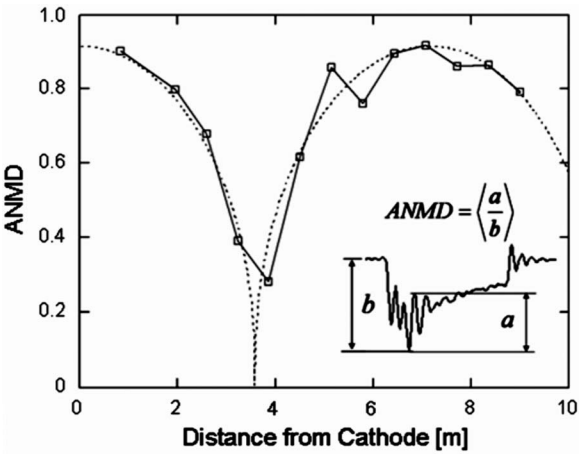

FIG. 8. Evolution of beam modulation as a function of distance traveled. Average normalized modulation depth (ANMD) is a measure of modulation strength relative to peak beam current. The dashed line is a fit to experimental data; null point in the fit was used to determine sound speed in the UMER beam [8].

calculated from formulas given in Ref. [2]. Using the measured value of the amplification factor, an approximate pulse-forming line signal can be deduced (Fig. 6) by calculating the beam current from Eq. (2) and comparing the calculated trace to the observed traces for various values of the bias voltage (Fig. 7). The inferred pulse-forming line signal shows a small amount of ringing at the leading edge of the pulse, and droop across the remainder of the pulse, as well as an apparent reflection at the falling edge of the pulse. All of these are features typically seen in pulsed power systems, and are unremarkable unless amplified, as can occur in the

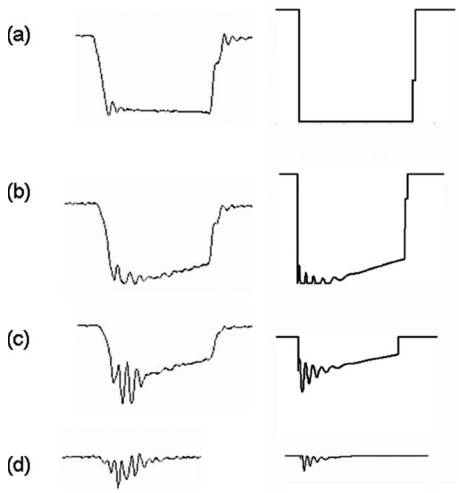

FIG. 7. Experimental beam pulse shapes measured in UMER for various values of bias voltage (left), compared to theoretical beam pulse shapes calculated from the inferred pulse-forming line pulse shape of Fig. 6 (right). Traces shown for space charge limited operation (a), transitional operation (b), triode amplification mode (c), and just before cutoff (d). Experimental traces show that the beam has undergone longitudinal expansion, increasing the rise and fall times of the pulse. Longitudinal expansion was not included in the theoretical calculations [8].

UMER gun. Unfortunately, the pulser was damaged before direct measurements were made for comparison to Fig. 6. The replacement pulser produced noticeably different beam modulation, suggesting a change in the voltage pulse shape applied across the cathode-grid gap. Recent direct measurements of this voltage with the new pulser show a waveform which is significantly different from that of Fig. 6, as expected [34]. However, the measurements indicate that the new pulser also exhibits ringing, reflection, and (in the reflection) droop.

As described in Sec. II, modulation of this type in gridded guns consists almost entirely of density modulation; in the case of the UMER gun, the strength of the current modulation is approximately $\eta=0.41$, compared to a velocity modulation strength of approximately $\delta=0.000\ 15$ [8].

The traces shown in Fig. 5 and the experimental traces shown in Fig. 7 were all measured at a single location on UMER; on closer inspection, the beam modulation was found to be a function of distance traveled along the beam line. The strength of the modulation was found to decrease over the first 3.2 m of the beam line, then to increase over the next 3.2 m, and finally to decrease again over the remaining 3 m. To quantify this variation, the maximum peak-to-peak modulation signal strength was measured for each data trace, and divided by the peak signal strength in the wave form. Finally, the values measured from each of the four plates of each BPM were averaged to give an "average normalized modulation depth" (ANMD) at each BPM location. The ANMD was plotted as a function of distance from the cathode, as shown in Fig. 8 for one set of operating conditions. By analogy with the evolution of discrete density perturbations, it was hypothesized that the initial modulation had formed a forward-traveling fast wave and a backward-traveling slow wave, each of which retained the shape of the initial modulation. The modulation is assumed to be of the form

$$A(t,z) = \cos(\omega t - kz) + \cos(\omega t + kz). \tag{30}$$

In this equation, $t = \frac{s}{c\beta}$ is the time it took the beam to travel a distance s along the beamline, and z is the position in the beam along which the fast and slow waves are traveling. For a modulation with frequency f observed in the lab, the wave number k has the value $\frac{2\pi f}{c\beta}$. The phase velocity of the fast and slow waves is then

$$v_p = \pm \frac{\omega}{k} = \pm \frac{\omega c \beta}{2\pi f}. \tag{31}$$

The frequency of modulation f was measured to be approximately 115 MHz. The angular frequency ω could be determined by the location of the null in the curves of Fig. 8; for the operating condition shown, this value was 2.64×10^7 s^{-1}. As a result, the phase velocity of the hypothesized fast and slow waves was determined to be $\pm 2.19 \times 10^6$ m/s for the operating condition shown. For comparison to theory, the sound speed was calculated from Eq. (4) and found to be $\pm 1.65 \times 10^6$ m/s when α is taken to be zero. However, Eq. (4) assumes a small-amplitude space charge wave propagating through a uniform background charge density λ_0, and neither of these conditions holds in this experiment. The beam current used to calculate the theoretical value was taken from beam current traces measured at the Bergoz current monitor 63 cm from the cathode, but because of the presence of the beam modulation and the unusual shape of the underlying beam, the average value of the unmodulated beam current in the location of the modulation could only be estimated. In addition, the strength of the beam modulation in general was not small compared to the background beam current. In this case, it is reasonable that Eq. (4) might underestimate the sound speed.

Following the precedent of the previous section, we will now consider a simplified version of this scenario from a theoretical perspective. We assume a continuous cosine modulation of an infinitely-long intense beam on which no other structure is present. We begin by noting that the BPMs and the Bergoz fast current transformers [35] used to observe the beam modulation in UMER detect beam current, rather than the beam velocity or charge density. However, we can see from Eqs. (11) and (12) that for a beam with no initial velocity modulation, the current and density in an intense beam are directly proportional. As before, we note that the initial potential energy stored in the density-modulated beam is

$$U_i = \frac{\eta g' \lambda_0^2}{2\pi\varepsilon_0} \int_{z_1}^{z_2} h(z) dz. \tag{32}$$

Let us assume the initial density perturbation to be a continuous cosine modulation of the form

$$h[z] = \cos[kz]. \tag{33}$$

This initial modulation may be thought of as the superposition of the fast and slow waves, which have not yet separated (Fig. 9). The fast and slow density waves are of the same sign, and therefore add constructively. The initial stored potential energy associated with this modulation is

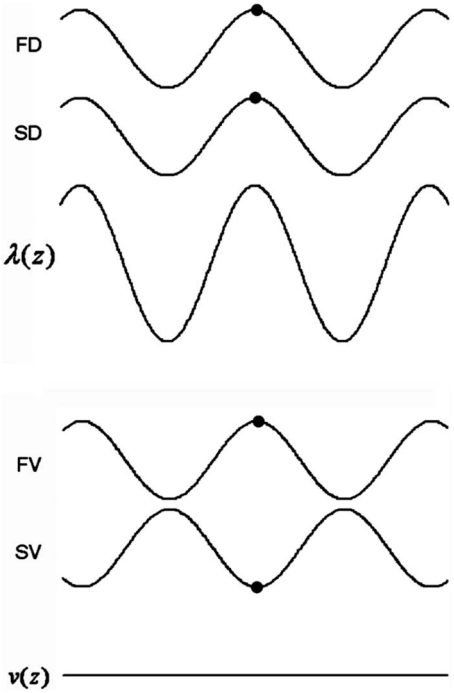

FIG. 9. Initial configuration of beam at $s=0$: density modulated. Fast density wave (FD) and slow density wave (SD) add constructively, while fast velocity wave (FV) and slow velocity wave (SV) add destructively.

$$U_i = \frac{\eta g' \lambda_0^2}{2\pi\varepsilon_0 k} \sin kz \Big|_{z_1}^{z_2}. \tag{34}$$

If this is integrated over all of our infinitely-long beam, we find that there is no extra potential energy stored in the beam due to the modulation. In this way, the continuously modulated case is different from the discretely modulated case. However, while there is no net additional stored potential energy in the beam, the modulation creates regions of high and low potential energy; wherever $\lambda > \lambda_0$, the local potential energy density exceeds the average value in the beam, and wherever $\lambda < \lambda_0$, the local potential energy density is less than the average value in the beam. Thus the beam is modulated in density, which causes it to be modulated in potential energy. In contrast, the fast and slow velocity waves are of opposite sign, so that their contributions cancel and the beam everywhere returns to its average value of velocity, and therefore of kinetic energy (Fig. 9).

The fast and slow waves produced by the initial density modulation will travel past each other, and the beam will reach a condition where the density waves are now out of phase (Fig. 10). As a result, the fast and slow density waves will add to zero, and the perturbed potential energy calculated from Eq. (21) will be zero everywhere. However, the signs of the fast and slow velocity waves are opposite, and so they will now sum constructively; the beam has become velocity modulated. This will occur after the (coasting) beam has traveled a distance of

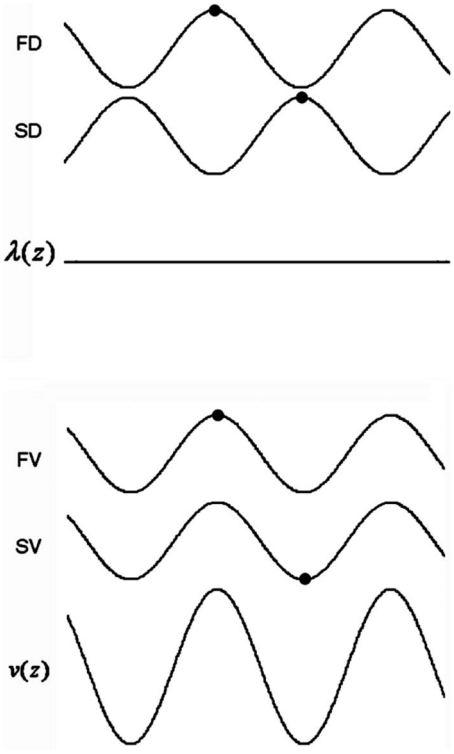

FIG. 10. Intermediate configuration of beam at $s=\frac{Lv_0}{4c_0}$: velocity modulated. Fast density wave (FD) and slow density wave (SD) add destructively, while fast velocity wave (FV) and slow velocity wave (SV) add constructively.

$$s = \frac{Lv_0}{4c_0}, \tag{35}$$

where L is the wavelength of the initial density modulation. Note that the peak of the velocity modulation occurs halfway between the old locations of the peak and trough in the density modulation. If the beam is assumed to be axially symmetric, the full conversion of potential energy to kinetic energy can easily be shown for particles whose positions and velocities are constrained to lie along the axis. The difference in potential energy between the peak and trough of the original density modulation was,

$$\Delta U = \int_{\text{trough}}^{\text{peak}} qE_z dz = \frac{gq}{2\pi\varepsilon_0\gamma^2}\eta\lambda_0, \tag{36}$$

where E_z is the longitudinal electric field of Eq. (15) and $2\eta\lambda_0$ is the difference in density between peak and trough. The peak kinetic energy in the velocity modulation, calculated from Eq. (13) for the case of constructive interference between the fast and slow velocity waves, is

$$T = \frac{1}{2}m[2\eta c_0]^2 = \frac{gq}{2\pi\varepsilon_0\gamma^5}\eta\lambda_0. \tag{37}$$

Equations (36) and (37) are equal in the nonrelativistic limit, showing that there is full conversion of potential energy into kinetic energy. Allowing the beam to propagate to $s=\frac{Lv_0}{2c_0}$ will allow the density modulation to reform and the velocity modulation to disappear (Fig. 11).

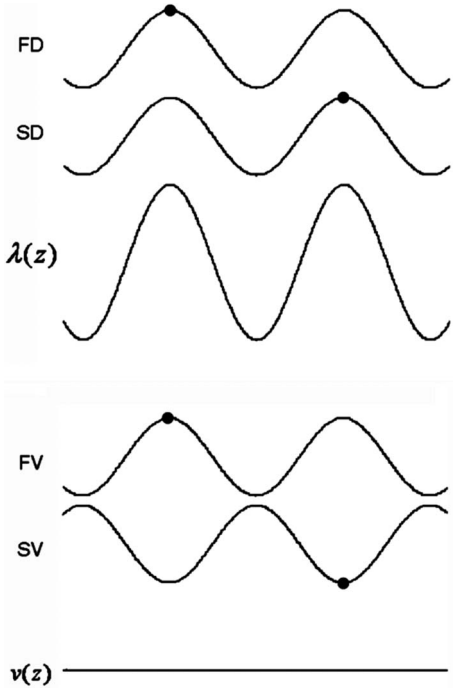

FIG. 11. Final configuration of beam at $s=\frac{Lv_0}{2c_0}$: density modulated. Fast density (FD) wave and slow density (SD) wave add constructively, while fast velocity (FV) wave and slow velocity (SV) wave add destructively.

D. Observations on energy conversion

So far, we have looked at two examples of density modulation in intense beams, and the wave propagation and energy transfer which results. In the case of a single, unipolar density perturbation, fast and slow velocity and density waves are launched. These waves retain the shape of the initial perturbation and continue propagating forever if they do not encounter the beam ends [36] or other effects such as resistive channels [37,38]. The perturbation (and resulting waves) store extra net energy in the beam, compared to an unperturbed beam. This extra net energy is stored in the form of potential energy due to the accumulation of additional charge in the perturbation (or waves), and in the form of kinetic energy due to the accumulation of additional mass in the perturbation (or waves). Most importantly there is no oscillation between density and velocity modulation, and stored energy is not converted between potential and kinetic forms once the fast and slow waves have separated.

In the case of a continuous modulation, fast and slow waves are also launched, which retain the shape of the initial modulation. However, the initial modulation (and resulting waves) do not store extra net energy in the beam, compared to an unmodulated beam. However, the initial modulation contains alternating, adjacent regions storing higher and lower potential energy than the beam's average value. This local potential energy imbalance can be seen as driving an

TABLE I. Properties of the two types of modulation discussed in this paper.

	Discrete modulation	Continuous modulation
Shape	Unipolar	Bipolar
Extra mass and charge?	Yes	No
Additional net energy stored?	Yes	No
Potential ↔ kinetic conversion?	No	Yes
Density ↔ velocity modulation conversion?	No	Yes

oscillation between the density-modulated state (in which energy is stored as potential energy) and the velocity-modulated state (in which energy is stored as kinetic energy). These results are summarized in Table I. The discrete-perturbation case and the continuous-modulation case represent opposite extremes; other cases may fall between these extremes and exhibit a mix of their characteristics. Note that to produce any oscillation and conversion between potential and kinetic energy in density-modulated beams, the initial modulating signal must be bipolar, with regions where $\lambda_1 > \lambda_0$ and other regions where $\lambda_1 < \lambda_0$. For full conversion between density modulation and velocity modulation, the modulating signal must be symmetrical about the $\lambda_1 = 0$ axis. Also note that the analysis used here for sinusoidally modulated beams can be applied to any periodic modulation through the use of the Fourier series.

IV. CONSEQUENCES AND APPLICATIONS

The dynamics discussed above can have a wide range of consequences and applications for accelerator systems. For example, space-charge waves are widely thought to have potential as a beam diagnostic to measure quantities that appear in the sound speed [22,23,39]. The presence of two counterpropagating waves of similar shape will lead to interference effects [8], which may enhance the precision of such techniques. In addition, space charge waves may be inadvertently launched in systems designed for heavy ion fusion [40]. Beam modulation has always played a role in the production of electromagnetic radiation. Generally, this involved both modulation and radiation entirely at nonrelativistic energies, as in traditional klystrons [2], or entirely at highly relativistic energies, as in the free-electron laser [41]. Acceleration to high γ is often desired specifically to avoid space-charge issues of the type discussed in this paper, since the sound speed decreases and because beams become less intense (transversely) as γ is increased. However, there has been some interest in systems which modulate the beam at the cathode, accelerate the modulated beam, and then have it interact with changing boundary conditions or fields to generate radiation [3–6,42–44]. In principle, this technique could allow more compact light sources, or light sources which operate in regions of the spectrum (such as the terahertz region) where sources are weak or nonexistent. However, systems which produce intense, density-modulated beams at the cathode will exhibit some of the effects described in this paper. Specifically, the density modulation will launch fast and slow waves. For producing radiation, continuous or quasicontinuous operation is desired to give finer control over the wavelength of the output radiation. But continuous density modulation will undergo the oscillation between density modulation and velocity modulation described above. This oscillation will occur faster at high current levels and at small beam velocities. If the beam were allowed to evolve without acceleration, the density modulation—which is necessary for the radiative mechanism—would completely disappear. To prevent this, a premodulated light source immediately accelerates the density-modulated beam as soon as it leaves the cathode. If this is done quickly enough, the sound speed in the beam will quickly decrease towards zero. All beams of interest begin their lives as intense beams, but the acceleration described here will quickly cause the beam to no longer be intense, but rather (transversely) emittance dominated [1]. As emittance becomes more important, the analysis presented in this paper no longer applies.

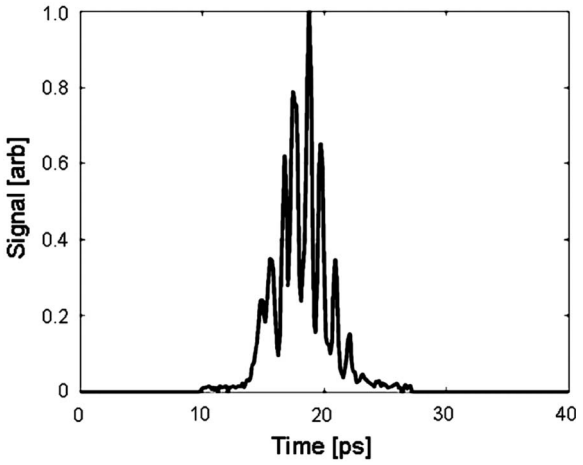

FIG. 12. Cross-correlator measurement example of modulated drive laser pulse.

An experiment along these lines was recently performed at Brookhaven National Laboratory using their Source Development Laboratory's Deep Ultra-Violet Free Electron Laser (DUV-FEL) facility [3–6,45]. When the machine is used as an FEL, a drive laser produces a 5–10 ps pulse of electrons at a copper cathode through photoemission. The electrons are then accelerated to approximately 250 MeV, at which point they enter a wiggler to produce coherent light.

The purpose of exploring electron beam density modulation drove a slightly different configuration of the accelerator system. In this case, the drive laser pulse was coded with terahertz modulations in order to serve as a switch at the photocathode. A scanning cross correlator was used to measure the time profile of the laser pulse [46]. Measurements show several subpicosecond pulses separated by spaces of similar length (Fig. 12). Since photoemission from copper is prompt (subfemtosecond) [47], electrons will be emitted

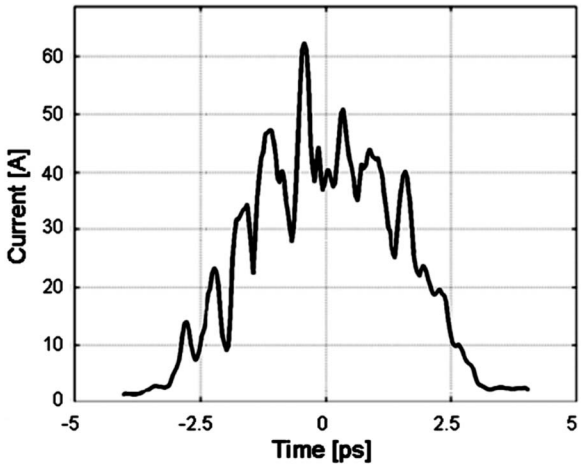

FIG. 13. Projection of longitudinal phase space onto time coordinate. Note washout compared to the laser pulse in Fig. 12.

with a temporal profile which closely resembles that of the incident laser pulse. Initially, the electron beam is strongly dominated by space charge forces, which are mitigated as energy increases.

After the electron beam is accelerated, the longitudinal phase space can be measured by tomographic reconstruction [48]. This reconstruction is formed by taking several one-dimensional projections of the two-dimensional longitudinal phase space. The projections are formed by placing an energy chirp on the beam and using a spectrometer (magnetic dipole) to measure the projection of the chirp-modified phase space on the energy axis. The chirp is varied by changing either the amplitude or the phase.

Any density modulation present on an electron beam will affect the nature of radiation it might emit. If some mechanism causes a single electron to emit a specific wavelength of light, a bunch train of electrons separated by that wavelength would emit in such a way that their electric fields would add in phase. The result would be enhanced emission at that wavelength, with the resultant electric field proportional to the square of the number of electrons in the beam. If on the other hand, all of the electrons were randomly distributed throughout the beam, the electric fields would add incoherently, and the resultant electric field would be directly proportional to the number of electrons in the beam. The coherent emission could serve as a source of light, as well as an electron beam diagnostic. This mechanism is employed in many of the devices listed previously.

At the DUV-FEL, a mirror can be inserted into the beam pipe such that it intercepts the electron beam at an angle. At the boundary between the mirror and the vacuum, the beam produces transition radiation which is reflected out of the accelerator system. This light is transported to a single element bolometer that was equipped with several band-pass filters. Recording the amount of energy measured with each filter in place gives an idea of how much energy falls into each band from the modulated electron beam.

After acceleration, the initial density modulation coded on the electron beam does not appear intact. In fact, the beam exhibits some conversion between density modulation and

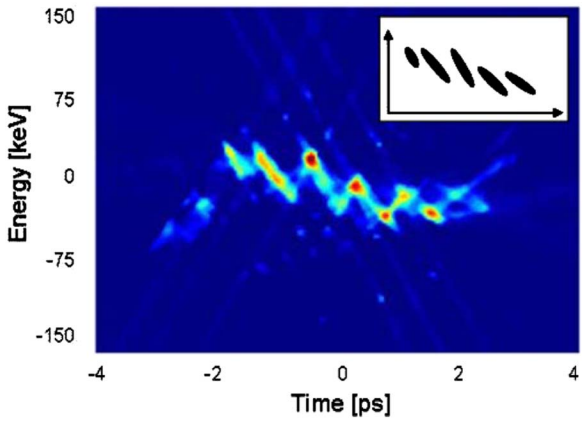

FIG. 14. (Color online) Reconstructed longitudinal phase space. The inset shows orientation of main microbunches.

kinetic energy modulation. Examining the reconstructed longitudinal phase space reveals that a projection onto the position coordinate results in a partially washed out density profile compared to the initial laser pulse (Fig. 13). However, the bunches are separated by voids in phase space (Fig. 14).

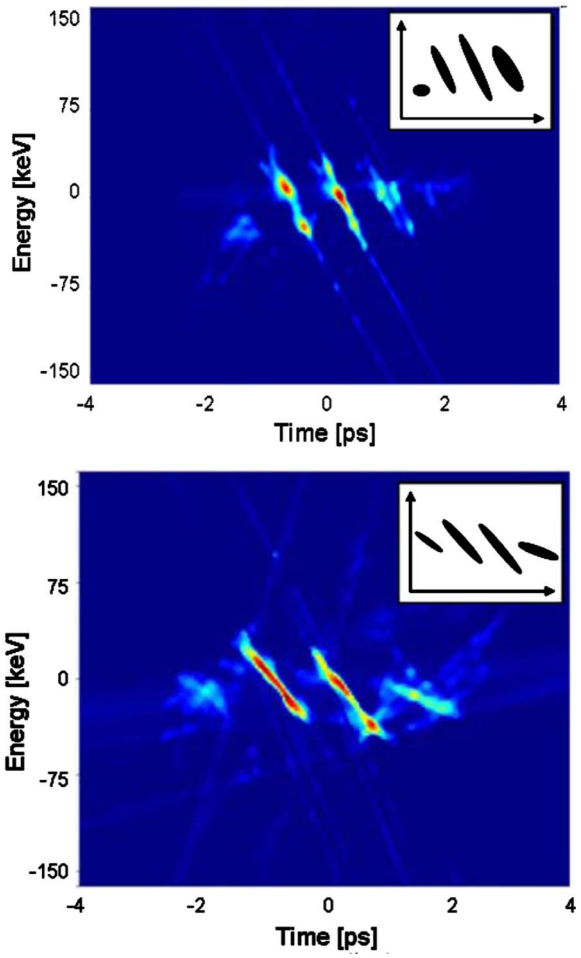

FIG. 15. (Color online) Reconstructed longitudinal phase space for beams with total bunch charge of 20 pC (top) and 160 pC (bottom). Insets show orientation of main microbunches.

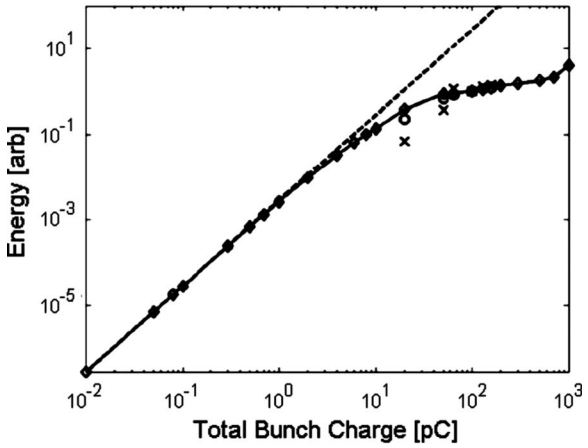

FIG. 16. Total (unfiltered) terahertz energy generated by a modulated electron beam based on calculations from PARMELA simulations (diamond), calculations from tomographic reconstructions (cross), and actual bolometer measurements (circle). The dashed line is a reference defined by a quadratic dependence on charge, which is expected when space charge forces are negligible [6].

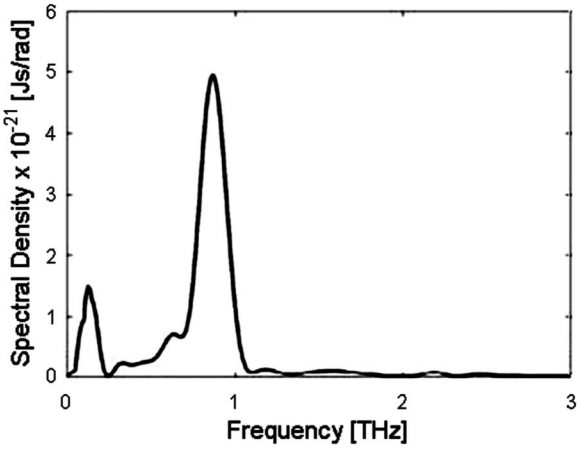

FIG. 17. Reconstructed terahertz spectrum [6].

As the bunch charge increases, the density modulation washes out further, and the angle of rotation in phase space is increased. A good example of this is shown in Fig. 15, where the longitudinal phase space diagrams correspond to bunch charges of 20 and 160 pC, respectively. This is an indication that the transfer between density and energy modulation is a result of space charge.

Therefore, as the charge increases, the amount of terahertz light produced is a function of both the total bunch charge and the density modulation of the electron beam. Increasing the amount of charge at very low total charge levels causes an increase in terahertz light with the square of the charge. The reason for this is that space charge forces are not strong enough to cause density washout. As the charge increases further, density washout begins to occur. The point at which this occurs is dependent on the derivative of the line charge density across the profile. The result is that as charge increases, the amount of terahertz light produced within a specific band can actually decrease. Eventually, the density washout will be nearly complete, and the total light produced will again increase, except only linearly with charge. This departure from the quadratic increase is demonstrated in Fig. 16.

The spectra of the radiated light can be calculated from the longitudinal phase space for each case. In order to do this, the light emitted at the mirror is calculated along with the effect of the light transport system. For comparison, the effect of the passband filters can be applied to the spectra, and compared to the values measured at the bolometer. An example of a calculated spectrum is shown in Fig. 17. Bolometer measurements, expressed in terms of an enhancement factor relative to an unmodulated beam, are shown in Fig. 18.

Note that the conversion between density modulation and velocity modulation may also have detrimental effects when the modulation is unwanted. Unwanted density modulation may occur in photoinjector systems where the applied drive laser contains unintended structure. If this density modulation remains on the beam, it may be a source of coherent radiation when interacting with fields or boundary conditions. However, if it is allowed to convert into velocity modulation, it may resurface later in the beamline due to dispersion. These matters are of importance for designers of photoinjector systems.

V. CONCLUSIONS

In this paper, we have discussed the generation, evolution, and consequences of density modulation of intense, nonrelativistic beams. Density modulation may be produced in a number of ways, including by photomodulation or through the use of gridded electron guns. Depending on the structure of the modulation, the density modulation may convert in part or in whole to velocity modulation. This represents a conversion of the energy stored in the beam modulation from

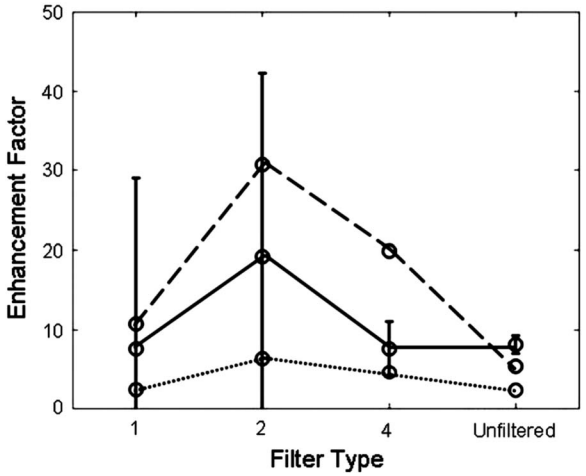

FIG. 18. Enhancement factor for different passband filters centered at (1) 0.703 THz, (2) 0.9678 THz and (4) 1.56 THz, for measured (solid), simulated (dashed), and calculated (dotted) results. Vertical lines represent error bars on experimental measurements.

potential energy to kinetic energy. The resulting space charge waves have potential for use as diagnostics. Although the dynamics described here assume intense, nonrelativistic beams, they may still have consequences for more conventional high-energy beams.

ACKNOWLEDGMENTS

The authors would like to thank M. Reiser, Y. Cui, and I. Haber for valuable discussions on the subject of intense beams. This work was funded by the Department of Energy, the Office of Naval Research, the Army Research Laboratory, and the Directed Energy Professional Society. Portions of this work were performed under the auspices of the U.S. Department of Energy by the University of California, Lawrence Livermore National Laboratory under Contract No. W-7405-Eng-48.

[1] P. G. O'Shea, M. Reiser, R. A. Kishek, S. Bernal, H. Li, M. Preussner, V. Yun, Y. Cui, W. Zhang, Y. Zou, T. Godlove, D. Kehne, P. Haldemann, and I. Haber, Nucl. Instrum. Methods Phys. Res. A **464**, 646 (2001).

[2] K. R. Spangenberg, *Vacuum Tubes* (McGraw-Hill, New York, 1948).

[3] J. G. Neumann, P. G. O'Shea, D. Demske, W. S. Graves, B. Sheehy, H. Loos, and G. L. Carr, Nucl. Instrum. Methods Phys. Res. A **507**, 498 (2003).

[4] J. Neumann, P. G. O'Shea, D. Demske, R. Fiorito, G. L. Carr, H. Loos, T. Shaftan, B. Sheehy, and Z. Wu, in *Proceedings of the 2003 Particle Accelerator Conference*, Portland, Oregon (IEEE, New York, 2003).

[5] J. Neumann, R. Fiorito, H. Freund, P. O'Shea, G. L. Carr, H. Loos, T. Shaftan, B. Sheehy, Y. Shen, and Z. Wu, in *Proceedings of the 2004 Free-Electron Laser Conference*, Trieste, Italy, 2004 (http://accelconf.web.cern.ch/accelconf/f04/papers/WEBOS02/WEBOS02.PDF).

[6] J. G. Neumann, Ph.D. thesis, University of Maryland, College Park, 2004.

[7] J. G. Neumann, J. R. Harris, B. Quinn, and P. G. O'Shea, Rev. Sci. Instrum. **76**, 033303 (2005).

[8] J. R. Harris, Ph.D. thesis, University of Maryland, College Park, 2005.

[9] J. R. Harris, J. G. Neumann, and P. G. O'Shea, J. Appl. Phys. **99**, 093306 (2005).

[10] K. Tian, Y. Zou, Y. Cui, Y. Huo, M. Reiser, I. Haber, R. Kishek, and P. G. O'Shea, in *Proceedings of the 2005 Particle Accelerator Conference*, Knoxville, TN, 2005 (http://accelconf.web.cern.ch/AccelConf/p05/PAPERS/TPAT067.PDF)

[11] J. R. Harris, J. G. Neumann, D. Feldman, R. Feldman, Y. Huo, B. Quinn, M. Reiser, and P. G. O'Shea, in *Proceedings of the 2005 particle Accelerator Conference*, Knoxville, TN, 2005 (http://ieexplore.ieee.org/xpls/abs_all.jsp?arnnumber=1590537)

[12] J. R. Harris, J. G. Neumann, and P. G. O'Shea, in *Proceedings of the 2005 Free-Electron Laser Conference*, Stanford, CA (http://accelconf.web.cern.ch/AccelConf/f05/PAPERS/THPP062.PDF)

[13] K. L. Jensen, D. W. Feldman, and P. G. O'Shea, Appl. Phys. Lett. **85**, 5448 (2004).

[14] K. Tian, Y. Zou, Y. Cui, I. Haber, R. A. Kishek, M. Reiser, and P. G. O'Shea, Phys. Rev. ST Accel. Beams **9**, 014201 (2006).

[15] D. Sutter (private communication).

[16] J. R. Harris and P. G. O'Shea, IEEE Trans. Electron Devices **53**, 2824 (2006).

[17] A. Valfells, D. W. Feldman, M. Virgo, P. G. O'Shea, and Y. Y. Lau, Phys. Plasmas **9**, 2377 (2002).

[18] D. H. Dowell, S. Joly, A. Loulergue, J. P. de Brion, and G. Haouat, Phys. Plasmas **4**, 3369 (1997).

[19] M. Reiser, *Theory and Design of Charged Particle Beams* (Wiley, New York, 1994).

[20] J. G. Wang, D. X. Wang, and M. Reiser, Phys. Rev. Lett. **71**, 1836 (1993).

[21] A. Faltens, E. P. Lee, and S. S. Rosenblum, J. Appl. Phys. **61**, 5219 (1987).

[22] J. G. Wang, H. Suk, D. X. Wang, and M. Reiser,Phys. Rev. Lett. **72**, 2029 (1994).

[23] J. G. Wang and M. Reiser, Rev. Sci. Instrum. **65**, 3444 (1994).

[24] J. G. Wang, E. Boggasch, P. Haldemann, D. Kehne, M. Reiser, T. Shea, and D. X. Wang, IEEE Trans. Electron Devices **37**, 2622, 1990.

[25] Y. Cui, Y. Zou, A. Valfells, M. Reiser, M. Walter, I. Haber, R. A. Kishek, S. Bernal, and P. G. O'Shea, Rev. Sci. Instrum. **75**, 2736 (2004).

[26] Y. Zou, Y. Cui, V. Yun, A. Valfells, R. A. Kishek, S. Bernal, I. Haber, M. Reiser, P. G. O'Shea, and J. G. Wang, Phys. Rev. ST Accel. Beams **5**, 072801 (2002).

[27] Y. Zou, Y. Cui, M. Reiser, and P. G. O'Shea, Phys. Rev. Lett. **94**, 134801 (2005).

[28] Y. Huo, M. S. thesis, University of Maryland, College Park, 2005.

[29] I. Haber (private communication).

[30] http://www.umer.umd.edu

[31] I. Haber, S. Bernal, R. A. Kishek, P. G. O'Shea, B. Quinn, M. Reiser, Y. Zou, A. Friedman, D. P. Grote, and J.-L. Vay, in *Proceedings of the 2003 Particle Accelerator Conference*, May 2003 (http://ieeexplore.ieee.org/xpls/abs.all.jsp?arnumber=1289192)

[32] J. R. Pierce, *Theory and Design of Electron Beams* (Van Nostrand, Princeton, 1954).

[33] B. Quinn, B. Beaudoin, S. Bernal, A. Diep, J. Harris, M. Holloway, D. Lamb, W. Lee, M. Glanzer, M. Quirus, M. Reiser, M. Walter, A. Valfells, R. Yun, and P. G. O'Shea, in *Proceedings of the 2003 Particle Accelerator Conference*, http://accelconf.web.cern.ch/AccelConf/p03/PAPERS/WPPB073.PDF

[34] B. Beaudoin http://www.umer.umd.edu/technicalnotes/2006/UMER-06-1114-BLB.pdf

[35] http://www.bergoz.com/fct/d-fct.htm

[36] J. G. Wang, D. X. Wang, H. Suk, and M. Reiser, Phys. Rev.

Lett. **74**, 3153 (1995).
[37] J. G. Wang, H. Suk, and M. Reiser, Phys. Rev. Lett. **79**, 1042 (1997).
[38] Y. Zou, J. G. Wang, H. Suk, and M. Reiser, Phys. Rev. Lett. **84**, 5138 (2000).
[39] F. M. Bieniosek, S. Eylon, A. Faltens, A. Friedman, J. W. Kwan, M. A. Leitner, A. W. Molvik, L. Prost, P. K. Roy, P. A. Seidl, and G. Westenkow, in *Proceedings of the 2004 International Symposium on Heavy Ion Inertial Fusion*, Princeton, NJ (2004).
[40] C. M. Celata *et al.*, Phys. Plasmas **10**, 5 (2003).
[41] P. G. O'Shea and H. P. Freund, Science **292**, 1853 (2001).
[42] E. G. Zaidman and M. A. Kodis, IEEE Trans. Electron Devices **38**, 2221 (1991).
[43] R. K. Parker, R. H. Abrams, B. G. Danly, and B. Levush, IEEE Trans. Microwave Theory Tech. **50**, 835–845 (2002).
[44] V. L. Granatstein, R. K. Parker, and C. M. Armstrong, Proc. IEEE **87**, 702 (1999).
[45] W. S. Graves, G. Carr, L. R. DiMauro, A. Doyuran, R. Heese, E. D. Johnson, S. Kronsky, C. Neuman, G. Rakowsky, J. Rose, J. Rothman, J. Rudati, T. Shaftan, B. Sheehy, J. Skaritka, L.-H. Yu, D. H. Dowell, and P. Emma, in *Proceedings of the 2001 Particle Accelerator Conference*, June 2001, Vol. 4 (http://ieeexplore.ieee.org/xpls./abs_ali.jsp?arnumber=987935).
[46] Henrik Loos, G. Lawrence Carr, Adnan Doyuran, William S. Graves, Eric D. Johnson, Samuel Krinsky, James Rose, Brian Sheehy, Timur V. Shaftan, John Skaritka, and Li-Hua Yu, in *Advanced Accelerator Conference: Tenth Workshop*, AIP Conf. Proc. No. 647 (AIP, Melville, 2002), p. 849.
[47] T. Tsang, Appl. Phys. Lett. **63**, 871 (1993).
[48] H. Loos, P. R. Bolton, J. E. Clendenin, D. H. Dowell, S. M. Gierman, C. G. Limborg, J. F. Schmerge, T. V. Shaftan, and B. Sheehy, Nucl. Instrum. Methods Phys. Res. A **528**, 189 (2004).